Mechanisms of the Intensity Dependent Refractive Index in Ultrastrongly Coupled Organic Cavity Polaritons

SAMUEL SCHWAB, [1] WILLIAM CHRISTOPHERSON, [1] MICHAEL CRESCIMANNO, [2] AND KENNETH SINGER[1,*]

[1] *Physics Department, Case Western Reserve University, 10900 Euclid Ave, Cleveland, OH 44106*
[2] *Physics Department, Youngstown State University, 1 University Plaza, Youngstown, OH 44555*
[*] *corresponding email*

Abstract: The nonlinear optical response of organic polaritonic matter has received increasing attention due to enhanced and controllable nonlinear response and potential for novel optical devices such as compact photon sources and optical and quantum information devices. Using z-scans over many wavelengths and incident powers we have studied the nonlinear response of ultrastrongly coupled organic cavity polaritons near the lower polariton band. We show that the highly enhanced nonlinear response arises from an intensity-dependent polaritonic resonant frequency. Consequently, we find that these z-scan data can only be described by several terms of a power series expansion in intensity whose respective contributions depend on power broadening and detuning from the lower polariton band. We further show that the nonlinear response can be quantitatively described by a three-level molecular quantum model coupled to the cavity in which saturation reduces the Rabi splitting, thus accounting for the lower polariton band's observed blueshift.

1. Introduction

Cavity polaritons are light-matter mixed states arising from coupling between excitonic matter and confined light fields [1]. Being part exciton and part photon, polaritons are highly tunable and have thus inspired an emerging field for potential chemical and quantum engineering applications [2–4]. Already, a plethora of classical and quantum phenomena ranging from angle-dependent amplification [5], parametric oscillation [6], and enhanced emission [7, 8] to single-quanta entanglement preservation [9], room-temperature out-of-equilibrium Bose-Einstein condensation [10], and superfluidity [11] have been found in polaritonic systems. Moreover, the ultrastrong coupling regime (where coupling energy compares to bandgap of material) opens up new avenues in tunability suitable for quantum and classical applications beyond the rotating-wave approximation [12, 13].

Cavity polaritons made from Wannier-Mott excitons found in semiconductor structures have been studied extensively and typically fall within the strong coupling regime for light-matter interactions [14]. In organic materials, the large binding energies of Frenkel excitons make ultrastrongly coupled polaritons easily attainable even with low-Q mirrors. Further, the ease of adjusting the exciton-photon coupling through mixing of organic dyes with polymers adds an additional and useful tunability [12, 15–17].

Exploration into the nonlinear optical properties of cavity polaritons has been fruitful. So far, enhanced and tunable third-harmonic generation [18–20] enhanced second harmonic generation [21], and novel four-wave mixing processes [22] have been explored. These works suggest that the nonlinear response is dictated by the polariton states, instead of the intuitive material resonant states. In this work, we further elaborate on this picture for the sum-over-states model by investigating ultrastrongly coupled organic polariton states extensively using a z-scan

technique over many pump wavelengths and powers. We measure a nearly 300-fold enhancement of the optical Kerr coefficient around the lower polariton (LP) resonance when compared to the bare excitonic film. We quantitatively show that optical saturation of the exciton reservoir leading to a blueshift of the LP band explains much of the experimentally observed behavior. A two-level Lorentzian model of the LP resonance indicates expected contributions of higher order nonlinear response to the intensity dependent refractive index. We find that a three-level quantum optics model of the organic molecule coupled to a cavity mode is able to quantitatively explain our observations. Notably, doing so with a three-level model only meaningfully introduces a single additional free parameter, the excited state mixing rate.

2. Background

Recently, polaritonic systems containing Frenkel excitons have been shown to exhibit strong blueshift in the LP when pumped around the threshold for creating a polariton condensate [23]. This shift has been primarily attributed to saturation and intermolecular energy migration. Although our experiments are at excitations below this condensate regime, we explore the effects of saturation on the detectable output of our samples in a z-scan configuration and bring insight into how saturation plays a pivotal role in this nonlinear optical regime.

To understand the effect of this resonant energy shift on the intensity dependent refractive index, we examine a two-level Lorentzian model comprised of a ground and excited state, in this case, the LP state, with associated population loss and dephasing rates γ and γ_2. We denote the product of the dipole matrix element connecting these two states and the exciting electric field by $E(t) = Ee^{-i\omega t} + c.c.$, with ω representing the input frequency. With this, one can solve the optical Bloch equations in the steady state, arriving at the solution for the density matrix element associated with a transition between ground and excited state. In the low intensity, low density limit, taking the real part of this solution gives the index of refraction,

$$Re(\rho_{01}) - 1 = n - 1 = \frac{\omega N d^2 \delta}{2\epsilon_0 c k_0 (\delta^2 + \gamma_2^2 + 4\frac{\gamma_2}{\gamma}E^2)} \Rightarrow U(G,\omega)\frac{\delta + \tau I}{(\delta + \tau I)^2 + \Gamma^2 + PI}, \quad (1)$$

where N represents the number density of the molecules, d their dipole matrix element, c the speed of light, k_0 is the vacuum wave vector, γ is the population relaxation rate, γ_2 is the decoherence rate, and $\delta = \omega - \omega_0$ is the detuning from resonance. We further simplify the expression using $U(G,\omega)$ the prefactor depending on the oscillator strength G, and anticipating its significance for this study, we introduce a blueshift parameter, τ, into the detuning, $\delta \rightarrow \delta + \tau I$, to give an intensity dependent blueshift. We also introduce Γ as a composite loss parameter and P as a power broadening parameter. Subsequently expanding Eq. 1 in powers of I reveals various orders of nonlinear optical response. Defining $\Delta n = n(I) - n(0)$,

$$\frac{\Delta n}{I} = n_2 + n_4 I + n_6 I^2 \quad (2)$$

where

$$n_2 = U(G,\omega)\frac{(\Gamma^2 - \delta^2)\tau - \delta P}{(\delta^2 + \Gamma^2)^2} \quad (3)$$

Expressions for n_4 and n_6 are given in supplemental information. These expressions indicate how the various nonlinear orders depend on the excitation wavelength. Note in the limit of small blueshift ($\tau \approx 0$) the expansion of the nonlinear index leads to sign alternation between nonlinear indices of increasing power as $n_2 < 0, n_4 > 0, n_6 < 0$. whereas at negative detuning for $\tau = 0$ the alternation is reverse, that is $n_2 > 0, n_4 < 0, n_6 > 0$. In this limit, this two-level model also

indicates a general qualitative trend; that with blueshift parameter (τ) each nonlinear term is not necessarily an odd function of the detuning from the resonance. This qualitative difference is salient below, as we use the three-level quantum model and compare with the experimental results.

We use this relationship in the investigation of the intensity dependent refractive index in our polaritonic samples, inferring contributions from n_2, n_4 and n_6. To convert both experimental measurements and numerical evaluations of the theory model into this form we followed the prescription in [24, 25].

3. Materials and Methods

The samples were fabricated on glass substrates by first thermally depositing Ag ($\sim$ 20nm) in a vacuum deposition chamber (Angstrom). Then, a solution of the organic dye molecule DCDHF-6V (absorption and photoluminescence shown in Fig. 1) and PMMA (2:1 mass ratio) was spun coat onto the silver, obtaining a sub-wavelength thickness of $\approx$135nm. The optical cavity was then finished by depositing the final silver layer ($\sim$ 20nm), yielding an overall quality factor for the cavity around 5. The linear optical dispersion of the entire structure is shown in Fig. 2 along with the wavelengths associated with the z-scan experiment. Our samples exhibit a Rabi splitting energy of 0.99 eV, placing our samples into the ultra-strong coupling regime.

Experiments were conducted using a parametric amplifier (TOPAS) pumped by a 200 fs laser system (Clark MXR) with repetition ration of 1 kHz. The closed and open aperture z-scan setup is depicted in the supplemental information in Fig. 13. The samples were illuminated with average powers of 1, 2, 4, 8, and 12 µW (peak intensity of 0.6, 1.2, 2.4, 4.8, and 7.2 GW/cm^2) and their associated open and closed aperture transmissions were recorded using Si large area biased photodetectors (Thorlabs Det100A2). The data were recorded every 50 µm over 20 mm centered around the focus of the Gaussian beam using a translation stage. The data were averaged over 30 pulses at each spatial point in addition to averaging over four total z-scans.

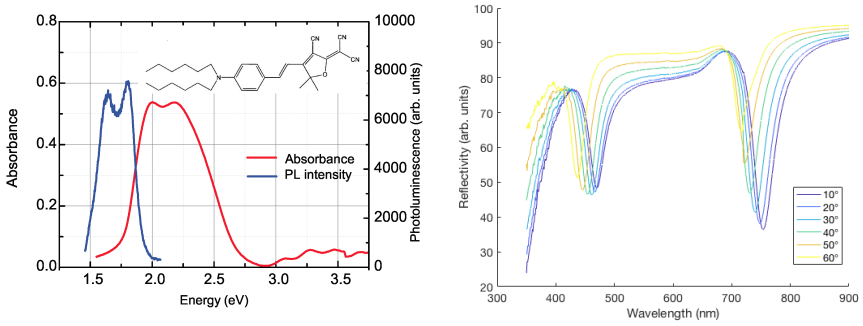

Fig. 1. Absorption (red) and photoluminescence (blue) of DCDHF-6V. Chemical structure shown in the inset (left). Reflectivity of sample at various angles of incidence (right)

4. Experimental Results

Z-scans were taken on both sides of the LP resonance and at various powers. The dominant feature of the open aperture was found to transition from diminished to enhanced transmission from the far-blue to the far-red side of the resonance, but in the intermediate region close to the polariton resonance we consistently measure a feature indicating a mixture of the two as shown in Fig. 3. This feature was present at all power levels, but its visibility for a specific pump

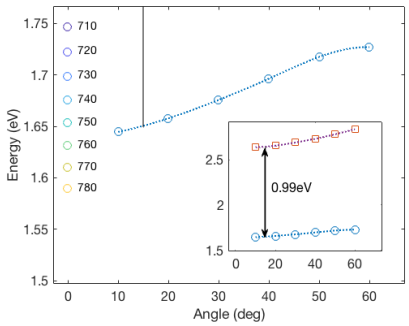

Fig. 2. Dispersion of polariton sample. Upper (red squares) and LP (blue circles) bands shown as inset, with Rabi splitting energy of about 1eV located at 15 degrees. Inset axes labels are same as main axes. The main figure shows the LP dispersion with the z-scan pump wavelengths from 710nm→780nm as dark to light circles at normal incidence.

wavelength depended on the incident power. We also measured a large response in the closed aperture detection arm indicating throughout a negative nonlinear refractive index for our system. To remove the effects of overall intensity change, we divide the closed aperture data and the open aperture data, also shown in Fig. 3. As a baseline, we also measured the nonlinear response of a thick film of DCDHF-6V (∼370 nm) (no mirrors and so no cavity polaritons) using the same preparation as the cavity polariton sample. We found the effective nonlinear index, n_2, at 680 nm of this thick film to be $1.58 \times 10^{-16}\ W/m^2$. Experimental open and closed/open aperture data for this thick film are included in the supplementary information.

We also investigated the power dependent nature of our responses to determine which high-order processes contribute to our data. Five average power levels were taken for all wavelengths from 710 to 780 nm. The overall transmission difference, from peak to valley, of the z-scan division are shown in the supplemental information, and the extracted $\Delta n/I$ are shown in Fig. 4. We see a general enhancement of the relative index change around the polariton resonance, but slightly blueshifted by about 10 nm. At higher powers this blueshift becomes larger. The nonlinear enhancement and evidence of higher-order effects is made apparent in the main panel of Fig. 4. The associated total index change ($\Delta n/I_0$) becomes diminished at higher power and indicates a high-order effect beyond $\chi^{(3)}$, of opposite sign. It is worth noting that the presence of curvature in this graphic necessitates the inclusion of an n_6 term. Otherwise this relationship would be linear for all observed wavelengths.

The right panel of Fig. 4 shows the extracted nonlinear indices which result from fitting the $\Delta n/I$ data to an order-two polynomial to match that of equation 3. We observe up to 300-fold enhancement of n_2 relative to the non-polaritonic result. In addition, there is an apparent alternation of overall sign in these extracted indices and a general symmetrical enhancement around the polariton resonance.

5. Discussion

Full Quantum Optics Model

Recently, it was shown in [19] that third harmonic generation into the polariton branches has a dispersive character indicating the active participation of the polariton state, and not the exciton. In the sum-over-(intermediate) states picture of third harmonic generation this fact indicates that the natural basis states for perturbation theory is not the exciton but the polaritons themselves. In a similar vein below, we explain the wavelength dependence of our more recent z-scan data also cannot be accommodated by a two level model of the dye exciton. Further we show that at

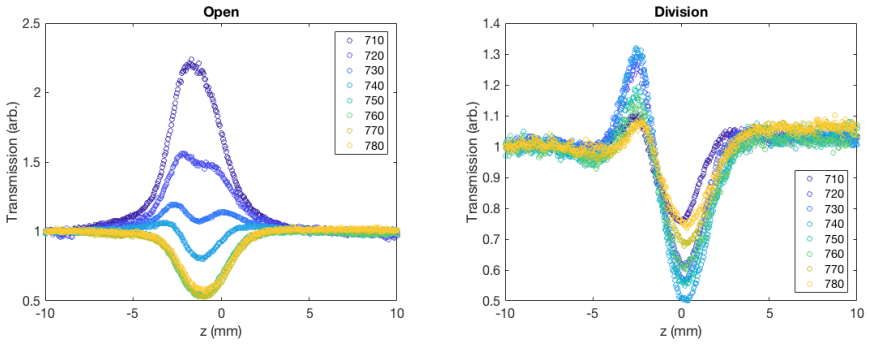

Fig. 3. Normal incidence open aperture (left) and closed/open aperture (right) z-scan data scanned at 4 μW average power at each respective wavelength.

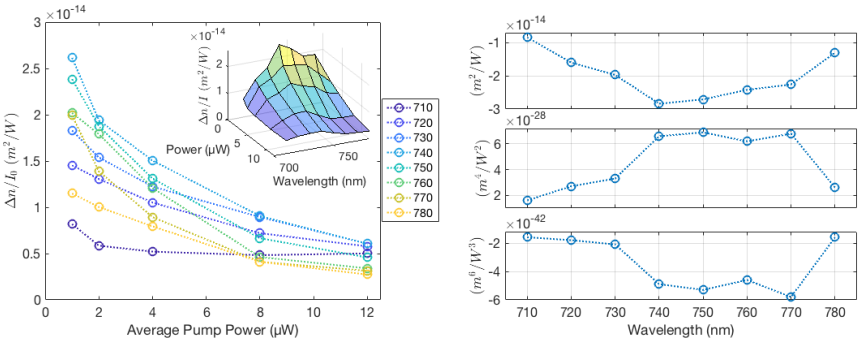

Fig. 4. Trends with intensity for change in index/intensity, where each line corresponds to a pump wavelength in nm for various input intensities. Inset shows surface plot of same data, but highlights the enhancement around the polariton resonance (left). Results from fitting process of the data on the left using an order two polynomial fit. These parameters are effective n_2, n_4, n_6 (top to bottom, respectively) of the system (right).

minimum, a three-level model is necessary to connect with the experimental results.

We note that, in general, three-level models appear to be minimal for capturing the linear and leading nonlinear phenomenology of most dyes [26–28]. Taking a cue from the absorption and photoluminescence curves of Fig. 1, our model for the organic dye on the left of Fig. 5 consists of a ground state connected by a large matrix element to an excited state centered at 600nm (~2.1eV, the exciton) that is coupled to a third state at 660nm (1.8eV, we call "PL", not shown) above the ground state that itself only slowly (radiatively) decays to the ground state. Further, in addition to the radiative processes between each the exciton or PL and the ground state, we include a fast non-radiative mixing between the PL state and exciton state. This describes significant rapid quenching of the exciton state into the PL state.

It is expected that the absorption and relaxation processes are fast compared to the excitation pulsewidth (see experimental section), thus it is sufficient to solve the associated three-level Bloch equations in steady state and use the excitonic coherences found in that limit to compute their contribution to the (complex, nonlinear) index of refraction for the dye layer. That index is then used in the transfer matrix modelling of the cavity polariton system. The matrix elements and relaxation process between the exciton, ground state, and PL state are assumed to be independent of the intensity. Note that to capture the nonlinear optical response of the system we must include

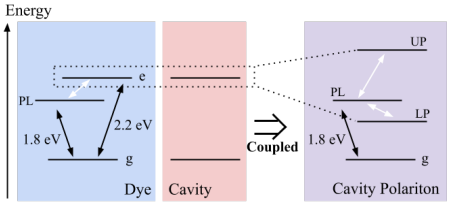

Fig. 5. The individual excitons co-operatively couple to the cavity fields. The dispersion in their collective optical response splits the nearby cavity resonance into two states, the upper ("UP") and lower ("LP") polaritons

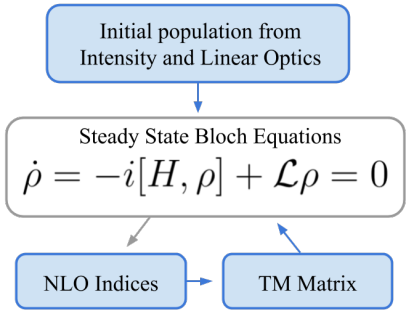

Fig. 6. General flow diagram showing how the numerical evaluation of our polariton system embedded in a z-scan setup takes place. The self consistent steady-state solution emerges from the final three blocks.

intensity-dependent changes in the index which critically modify (spectral location and depth of) the polariton states 'UP' and 'LP'. We do so at each given wavelength and incident intensity by iteratively updating the cavity fields after recalculating the index and transfer matrices until a self-consistent (stationary) cavity intensity is achieved. This process is diagrammatically shown in Fig. 6.

We numerically evaluate this model to emulate the z-scan experimental protocol. In brief, and as described in more detail below, the z-scan protocol [29, 30] consists of focusing a Gaussian laser field into a waist and translating the sample (the cavity polariton slide) through that waist. Downstream from the waist is a lens for collecting both the total light transmitted through the sample (the "open" z-scan signal) and that light that arrives behind the collection lens strictly on axis (the "closed" z-scan signal). The "open" signal indicates nonlinear absorption whereas "closed" channel passing through a nearly closed iris indicates a combination of nonlinear refraction and nonlinear absorption.

Some details of the numerical modeling are useful for understanding the meaning and limitations of our theory results described below. At each longitudinal sample location, z, we break the incident optical field into hundreds of concentric circular iso-intensity rings to capture the experimental beam intensity cross-section, evolving the field in each ring self-consistently as described earlier. To then form the expected "open" z-scan signal we simply sum the intensities emanating from each ring on the far side of the sample.

To compute an expected closed z-scan signal, at each sample location we use the same self-consistent solution of the transfer matricies to determine the exit phase retardation at each of the concentric rings individually. We then use the radial map of these phase retardations to determine an effective focal length of the intensity-induced lensing in the sample. Finally, this is combined with the optical geometry of the downstream part of the experiment (location and

focal length of the collection optics) to determine the light intercepted by the iris before the photodetector, yielding what we call the "closed" (channel) signal.

Qualitative analysis:

Much of the observed z-scan data delineating the nonlinear response in ultrastrongly coupled organic cavity polaritons can be understood as resulting from a single physical effect: the optical saturation of the dye. The remaining observations beyond this simple description then become experimental evidence for the necessity of including the effects of a third non-radiative level ("PL") in the underlying quantum optics model of the dye. We support these assertions below, first through a qualitative overview of the z-scan data, and then describe in detail the quantitative correspondence between the minimal three-level model for the dye and the zscan data.

The three main qualitative features and how they are the result of optical saturation for the open z-scan data for these ultrastrongly coupled organic cavity polaritons are:

1) SA- to RSA-like transition: As seen in Fig. 3, scanning in wavelength across the polariton resonance(s), the open z-scan data change by processes similar to saturable absorption (SA-like) (reduced nonlinear absorption) to reverse saturable absorption (RSA-like) (increased nonlinear absorption). The wavelength at which this transition occurs shifts blue with increasing intensity.

Saturation due to the brightening of the internal cavity optical fields reduces the cavity coupling. This reduces the vacuum Rabi frequency, reducing the gap between the polariton resonances. This causes the UP to move to longer wavelengths and the LP to shorter ('blueshift'), as shown in Fig. 7. Recall that at low intensities (linear optical regime), the polariton resonances increase the intracavity intensity. Thus, if blue detuned from the LP, during the intensity increase in a z-scan the LP moves towards the drive wavelength, resulting in SA-type behavior in the open z-scan channel. The same blueshift causes an intensity decrease when the LP is scanned at a red detuned wavelength, thus appearing RSA-like (see Fig. 8). If saturation dominates, then we would expect exactly the opposite behavior at the UP, which indeed is indicated by our experimental findings (not shown here). Note these findings cannot be reproduced by a wavelength-independent nonlinear index for the dye, because in that case both UP and LP would shift the same sense with intensity, as indicated in Eq. 3

2) Transition (M-shaped) feature in middle of SA-RSA transition: Also apparent from Fig. 3 is that the open aperture signal undergoes 're-entrant' behavior at wavelengths between the SA- and RSA-like ranges. With increasing optical power this re-entrant transition feature for the LP blueshifts in wavelength, broadens about z, and deepens in the middle.

As a result of the blueshift of the LP with intracavity intensity, the LP resonance center shifts so far that it passes to the blue of the excitation wavelength itself. In that case the absorption first decreases at $z \neq 0$ as the blueshift pulls the LP resonance towards it and then appears to increase as $z \rightarrow 0$ since there it continues to blueshift the LP so far that it starts going off resonance again *on the long wavelength side*. We note that there is a rich literature of such transition features [31–37] in open z-scan data, and in all cases the feature is a consequence of intensity dependent frequency pulling of an optical resonance of some sort. This picture also explains the increased broadening in z-scan co-ordinate, increased contrast with power, and implies that the same phenomenology should appear red of the UP, which we have also verified experimentally (not shown).

3) The RSA-like behavior in the open aperture data to the red of the LP persists far into red detuning, up to almost 100 nm beyond the LP.

This appears to not be a simple consequence of saturation; instead, we understand this behavior as consequent to the active participation of a third level in the quantum optics model for the dye. The participation of this third level through its rapid mixing with the exciton furnishes a longer lived set of metastable states that do not themselves directly lead to cavity pulling, but through excited state mixing, broaden the frequency response of the dye at high intensity. We directly,

quantitatively compare a 2- and 3-level model (with mixing) for the dye in Fig. 8 and Fig. 10.

Having related each observed open z-scan feature qualitatively to the dye quantum optics model, we now use it in the qualitative explanation of the closed z-scan signal, drawing attention to two defining features.

1) The sign of the effective n_2: The observed closed z-scan signal from the cavity LP correspond to a effective $n_2 < 0$ for all wavelengths and powers. The magnitude of the effect increases as one approaches the blueshifted LP center wavelength, and broadens (in z-scan co-ordinate z) with power.

This is a consequence of the fact that the LP is below the exciton. Even in a two level system, again as a consequence of power broadening/saturation, the first contribution to n_2 is expected to follow that of normal dispersion, being negative at detunings below the exciton and positive above, as indicated by our experimental findings at the UP (not included here). The broadening seen is consistent with the expected power dependence of the nonlinear response, and below we show that its observed blueshift with power is quantitatively consistent with that due to the depolarization of the dye associated with saturation in the cavity optical field.

2) The shape changes and dynamic range of the closed/open z-scan with power: As noted, the effective n_2 from the closed z-scan stays negative across the LP, but its magnitude changes with power differently at different detunings.

The sign of Δn does not tell the whole story. The magnitude of the Δn (i.e. proportional to the difference between the maximum and minimum closed/open zscsan signal during a trace) depends on detuning and fluence in such a way as to indicate the vital contribution of higher order nonlinear susceptibilities. As described in the experimental section (and as rendered from theory evaluation in Fig. 2 below), these changes are recorded as nonlinear contributions to the index, n_i, $i = 2, 4, 6$. Qualitatively all three of these show dependence on the detuning (from the polariton) that is a consequence of a blueshift, as indicated qualitatively by expanding out the expression for n_i from Eq.1.

Quantitative comparison:

Before making detailed quantitative comparisons between experiment and theory, we review briefly the parameter inputs we use to numerically evaluate the model. We show how every parameter but one (the mixing rate between the exciton and the PL states) is determined by the known geometry of the setup, measured powers, wavelengths and beam sizes and the dye's linear optical response.

It is convenient to separate the parameters into microscopic and macroscopic. The microscopic parameters refer to the quantities fixing the quantum optics model. As described earlier, they consist of exciton line center and effective width (measured for this dye in neat films by ellipsometry; see Ref. [15] about 600 nm line center and 1.5e4 GHz width), the gap (Stokes shift) between that state and the PL state, here fixed at 0.3eV below the exciton) and finally the excitonic dipole matrix element (also from Ref. [15], measured to be about 7.3 D). The single important unknown microscopic parameter subject to variation is the mixing rate between the exciton and the PL state. While there are potentially other microphysical parameters in the model (the decay rate of the PL state, the branching ratio of decays, the coherence decay rate between the excitonic state and the PL state, etc.) we find in fact that varying these other parameters (over reasonable ranges) does not materially effect the quantitative outcome of the polaritonic z-scan.

The macroscopic parameters are also all essentially fixed by linear optical measurements and well-characterized sample fabrication protocols. These include the layer thicknesses (deposition process control leaves those with variances below the 10% level) of the silver mirrors and the dye layer, the dye concentration with PMMA carrier, etc. The simple quantum optics model as described combined with the known dye density reproduces the (complex) linear optical index measured via ellipsometry, again, at the 10% level across the visible.

To model the optical response of the deposited silver mirrors we used the published bulk values

of $n + iK$ of Ref. [38]. We take throughout this manuscript our front and back silver layers to be 18 and 20 nm thick (resp.) and the dye layer to be 140 nm thick and the dye molecular number density of ~ 1.6 x 10^{21}/cc, which we note is consistent with the chemical preparation, but also proscribed by the measured vacuum Rabi splitting of the polaritons.

The result of modeling as one depolarizes the medium via saturation in an intense nearly resonant optical field is a reduction of the polariton gap. Generically this occurs by both branches trending towards the exciton transition frequency as one increases the power, and as shown below in Fig. 7 using the structure and dye concentration for our system, the UP and LP do not move by the same amount (compare Ref [39]).

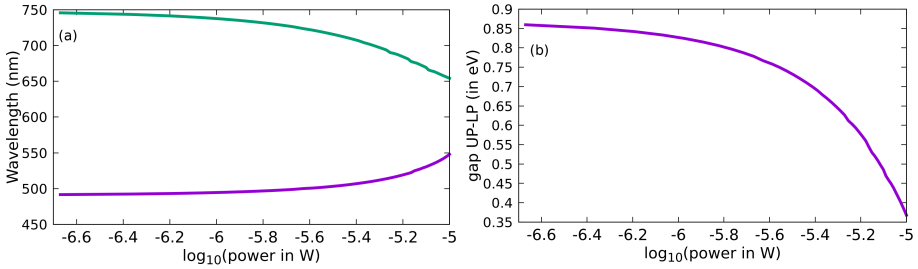

Fig. 7. The (a) change of the individual polariton branches for a sample at $z = 0$ and (b) rendered in terms of the polariton gap in eV as a function of the pump power, from evaluation of the quantum optics model and transfer matrix transport.

Similarly, as described in the experimental section, laser power, beam profile, z-scan optics chromatism and detection chain were well characterized and those measured parameters were used in connecting theory outputs (basically self-consistent nonlinear optical transfer matrices) to the associated open- and closed-signal channels.

Thus, with respect to the preceding discussion, we adjust only the exciton-PL mixing rate, showing below in Fig. 8 the modeled open channel output for two very different values of the mixing; 4 GHz (essentially the two-level reduction of our three-level numerical code) and 4 x 10^5 GHz. Note the overall similarity of the traces qualitatively, with each other and with the

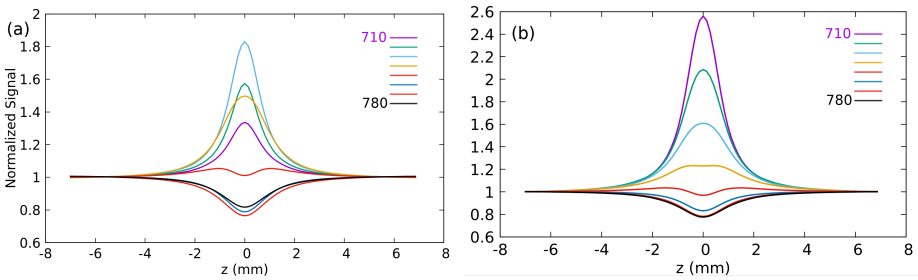

Fig. 8. Open zscan theory traces (710-780nm , each 10nm apart as in Fig. 3) for (a) small mixing (essentially a two state model for the dye) and (b) large mixing rate (=4 x 10^5 GHz between the exciton and the "PL" state), all other parameters the same. Compare with experimental Fig. 3(a), though these theory simulations used 4 μW of optical power.

experimental data of Fig. 3, with the greatest quantitative difference being the behavior of the traces at large red detunings.

Note the re-entrant transition trace in Fig. 8 at around 740 nm, a distinct qualitative correspondence with the experiment as seen in Fig. 3. We next plot as a function of power the

change in the wavelength at which the open z-scan transitions from SA-like to RSA-like, Fig. 9. The lines are theory curves and the points are experiment. This quantifies the distinct blueshift with power.

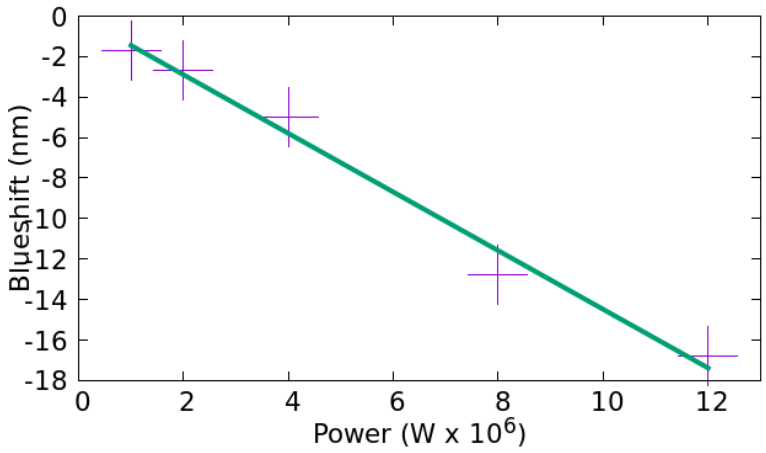

Fig. 9. The wavelength at which the open zscan at $z = 0$ has a transmission of 1 (matching large z) noticeably blueshifts with the power. Green curve is from evaluation of the theory and the points are experimental data. Note, this is not a fit.

Since we maintain that the non-Hermitian mixing rate between the PL and the exciton state is the only parameter we modify, we qualitatively compare experiment and theory in the long wavelength limit plotting the minimum of the theory open z-scan (i.e. at $z = 0$) as a function of red detuning for different choices that mixing rate.

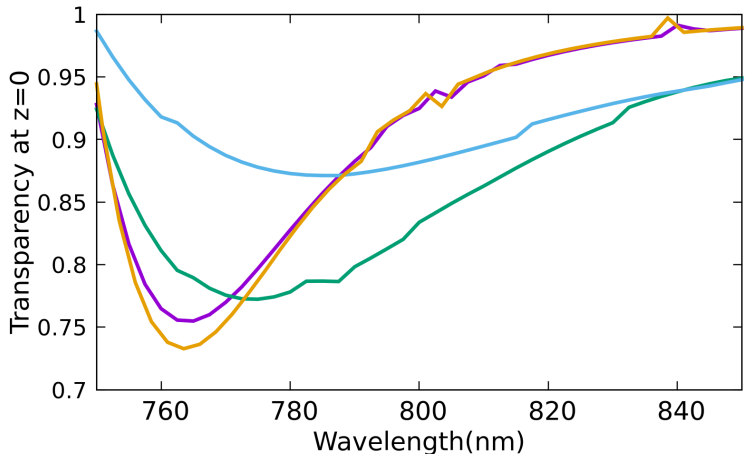

Fig. 10. Theory open zscan minima as a function of wavelength, all parameters the same except the mixing rate between the exciton and the "PL" state as described in the text. Power is 4 μW for all curves. The purple curve is the 2 state model (no mixing) the green is for a mixing rate of 4 x 10^5 GHz and the light blue curve is with a mixing rate of 8 x 10^5 GHz. The gold curve is the square of the two state (no mixing) model at half the power, showing that changing the power cannot explain the observed persistence of the additional nonlinear absorption red of the LP.

We henceforth adopt a mixing rate of 4.0x10^5 GHz in all the following numerical evaluations

of the theory model. The finding summarized in Fig. 10 provides evidence for the necessity of a three-level quantum optics model as a minimal one to understand the relevant contributions from the dye nonlinear optical properties, here seen in its NLO effect of the associated ultrastrongly coupled cavity polaritons.

This concludes our discussion of the quantitative comparison of theory and experiment for the open channel signal. We use the same model and parameters to now quantitatively compare the findings in the closed channel. It is perhaps easiest to interpret the ratio of the closed to open z-scan signal as most directly relating to the nonlinear index. As in the open channel signal, the overall dynamic range, shape (indicating the effective $n_2 < 0$ for all cases) are quite similar. One notes the qualitative correspondence of theory figure Fig. 11 with the data in Fig. 3 is not as compelling as between the theory and experiment in the open channel, as expected from the sensitivity of the closed/open z-scan simulation to both phase and intensity as compared to the open channel data. It is still worthwhile to quantitatively compare theory and experiment for

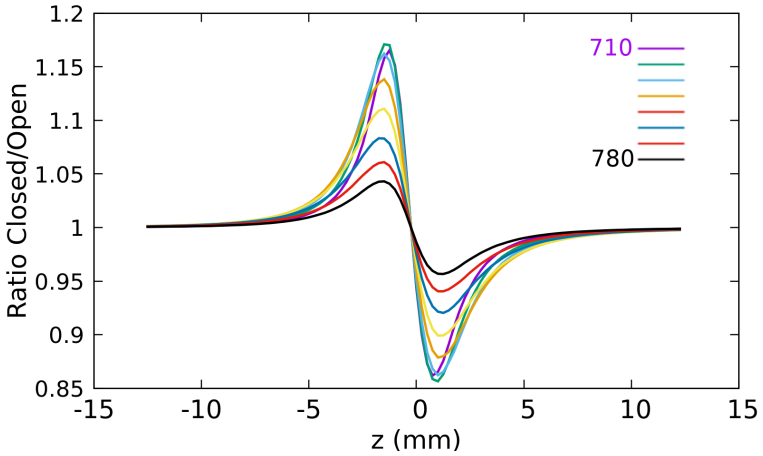

Fig. 11. Closed/Open Zscan theory curves. Parameters used identical to those used in making Fig 8(b). Compare with experimental data in Fig 3

these data by converting the simulation data to intensity-induced changes in the refractive index, via, for example, the procedure in Ref. [25]. As was done for Fig. 4, we numerically evaluate the total dynamic range (max-min) of the closed/open traces as a function of wavelength for the various powers. This is then used to compute the associated net refractive index change for the sample, as if it were a monolithic slab. The result of this procedure is shown in Fig. 12.

The shape change and the overall change in the width of the graphs at different powers is quite similar to that seen in experiment Fig. 4

6. Summary and Outlook

Our experimental findings and their accompanied theoretical elucidation using a straightforward three-level quantum optics model, with essentially a single adjustable parameter, indicates that for ultrastrongly coupled organic polaritons, the nonlinear refractive index is dominated by one main effect. Namely, the reduction of the vacuum Rabi frequency due to the saturation depolarization of the medium in the cavity's intense optical field. Such a process would also readily take place were there only two contributing levels. However, the experimentally measured behavior of the open aperture at large wavelengths (longer than the LP) is not explainable by a two-level model. Instead, that finding provides evidence for the necessity of including the third level in our quantum description of the dye.

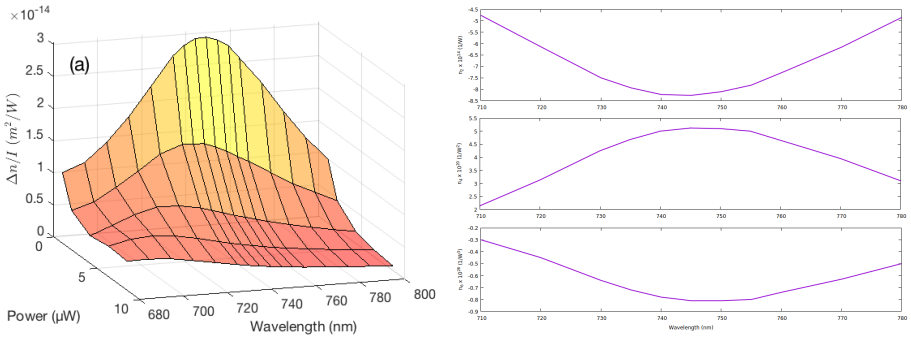

Fig. 12. (a) The theory-derived $\Delta n/I$ traces from theory closed/open theory. Parameters same as in Fig. 8(b). For (b) we converted the data in (a) into the intensity dependent contributions to the overall index of refraction of the sample. Compare with experimental Fig. 4.

Although that later point is not necessarily surprising, here we have done more by actually qualitatively and quantitatively connecting the underlying microphysical sources of the nonlinearities to those of the more complicated optical geometry. Further work is underway to delineate how dye-instrinsic higher-order nonlinear optical processes contribute to the observed z-scan signals.

Beyond being simply explanatory, we can use this model and understanding as a tool to predict and manipulate the nonlinear properties of multi-polariton systems, which may be of practical utility for optical switching and quantum information processing using polaritonic matter.

Funding

This work was supported by in part by the U.S. National Science Foundation (Grant DMR-1609077).

Acknowledgments

The authors acknowledge the use of the Materials for Opto/Electronics Research and Education Center (MORE) for sample preparation and characterization at Case Western Reserve University.

Disclosures

None of the authors of this paper has a financial or personal relationship with other people or organizations that could inappropriately influence or bias the content of the paper.

References

1. D. Sanvitto and S. Kéna-Cohen, "The road towards polaritonic devices," Nat. Mater. **15**, 1061–1073 (2016).
2. C. Schneider, K. Winkler, M. D. Fraser, M. Kamp, Y. Yamamoto, E. A. Ostrovskaya, and S. Höfling, "Exciton-polariton trapping and potential landscape engineering," Reports on Prog. Phys. **80** (2017).
3. I. Carusotto and C. Ciuti, "Quantum fluids of light," Rev. Mod. Phys. **85**, 299–366 (2013).
4. D. S. Dovzhenko, S. V. Ryabchuk, Y. P. Rakovich, and I. R. Nabiev, "Light-matter interaction in the strong coupling regime: Configurations, conditions, and applications," Nanoscale **10**, 3589–3605 (2018).
5. P. G. Savvidis, J. J. Baumberg, R. M. Stevenson, M. S. Skolnick, D. M. Whittaker, and J. S. Roberts, "Angle-resonant stimulated polariton amplifier," Phys. Rev. Lett. **84**, 1547–1550 (2000).
6. L. Ferrier, S. Pigeon, E. Wertz, M. Bamba, P. Senellart, I. Sagnes, A. Lemàtre, C. Ciuti, and J. Bloch, "Polariton parametric oscillation in a single micropillar cavity," Appl. Phys. Lett. **97** (2010).
7. D. Ballarini, M. De Giorgi, S. Gambino, G. Lerario, M. Mazzeo, A. Genco, G. Accorsi, C. Giansante, S. Colella, S. D'Agostino, P. Cazzato, D. Sanvitto, and G. Gigli, "Polariton-Induced Enhanced Emission from an Organic Dye under the Strong Coupling Regime," Adv. Opt. Mater. **2**, 1076–1081 (2014).

8. A. M. Berghuis, A. Halpin, Q. Le-Van, M. Ramezani, S. Wang, S. Murai, and J. Gómez Rivas, "Enhanced Delayed Fluorescence in Tetracene Crystals by Strong Light-Matter Coupling," Adv. Funct. Mater. **29**, 1901317 (2019).
9. Á. Cuevas, J. C. L. Carreño, B. Silva, M. De Giorgi, D. G. Suárez-Forero, C. S. Muñoz, A. Fieramosca, F. Cardano, L. Marrucci, V. Tasco, G. Biasiol, E. Del Valle, L. Dominici, D. Ballarini, G. Gigli, P. Mataloni, F. P. Laussy, F. Sciarrino, and D. Sanvitto, "First observation of the quantized exciton-polariton field and effect of interactions on a single polariton," Sci. Adv. **4**, eaao6814 (2018).
10. K. S. Daskalakis, S. A. Maier, R. Murray, and S. Kéna-Cohen, "Nonlinear interactions in an organic polariton condensate," Nat. Mater. **13**, 271–278 (2014).
11. G. Lerario, A. Fieramosca, F. Barachati, D. Ballarini, K. S. Daskalakis, L. Dominici, M. De Giorgi, S. A. Maier, G. Gigli, S. Kéna-Cohen, and D. Sanvitto, "Room-temperature superfluidity in a polariton condensate," Nat. Phys. **13**, 837–841 (2017).
12. A. Frisk Kockum, A. Miranowicz, S. De Liberato, S. Savasta, and F. Nori, "Ultrastrong coupling between light and matter," Nat. Rev. Phys. **1**, 19–40 (2019).
13. P. Forn-Díaz, L. Lamata, E. Rico, J. Kono, and E. Solano, "Ultrastrong coupling regimes of light-matter interaction," Rev. Mod. Phys. **91** (2019).
14. S. M. H. Luk, J. Keeling, F. M. Marchetti, M. H. Szymaska, and P. B. Littlewood, "Collective coherence in planar semiconductor microcavities," Semicond. Sci. Technol **22**, R1–R26 (2007).
15. B. Liu, P. Rai, J. Grezmak, R. J. Twieg, and K. D. Singer, "Coupling of exciton-polaritons in low-Q coupled microcavities beyond the rotating wave approximation," PHYSICAL REVIEW B **92**, 155301 (2015).
16. A. A. Anappara, S. De Liberato, A. Tredicucci, C. Ciuti, G. Biasiol, L. Sorba, and F. Beltram, "Signatures of the ultrastrong light-matter coupling regime," PHYSICAL REVIEW B **79** (2009).
17. S. Gambino, M. Mazzeo, A. Genco, O. Di Stefano, S. Savasta, S. Patanè, D. Ballarini, F. Mangione, G. Lerario, D. Sanvitto, and G. Gigli, "Exploring Light-Matter Interaction Phenomena under Ultrastrong Coupling Regime," ACS Photonics **1**, 1042–1048 (2014).
18. F. Barachati, J. Simon, Y. A. Getmanenko, S. Barlow, S. R. Marder, and S. Kéna-Cohen, "Tunable Third-Harmonic Generation from Polaritons in the Ultrastrong Coupling Regime," ACS Photonics **5**, 119–125 (2018).
19. B. Liu, M. Crescimanno, R. J. Twieg, and K. D. Singer, "Dispersion of Third-Harmonic Generation in Organic Cavity Polaritons," Adv. Opt. Mater. **7**, 1801682 (2019).
20. K. Wang, M. Seidel, K. Nagarajan, T. Chervy, C. Genet, and T. Ebbesen, "Large optical nonlinearity enhancement under electronic strong coupling," (2020).
21. T. Chervy, J. Xu, Y. Duan, C. Wang, L. Mager, M. Frerejean, J. A. W. Mü, P. Tinnemans, J. A. Hutchison, C. Genet, A. E. Rowan, T. Rasing, and T. W. Ebbesen, "High-Efficiency Second-Harmonic Generation from Hybrid Light-Matter States," Nano Lett. **16**, 7352–7356 (2016).
22. M. Romanelli, C. Leyder, J. P. Karr, E. Giacobino, and A. Bramati, "Four wave mixing oscillation in a semiconductor microcavity: Generation of two correlated polariton populations," Phys. Rev. Lett. **98**, 106401 (2007).
23. T. Yagafarov, D. Sannikov, A. Zasedatelev, K. Georgiou, A. Baranikov, O. Kyriienko, I. Shelykh, L. Gai, Z. Shen, D. Lidzey, and P. Lagoudakis, "Mechanisms of blueshifts in organic polariton condensates," Commun. Phys. **3**, 1–10 (2020).
24. K. S. Bindra, S. M. Oak, and K. C. Rustagi, "Intensity dependence of Z-scan in semiconductor-doped glasses for separation of third and fifth order contributions in the below band gap region," Opt. Commun. **168**, 219–225 (1999).
25. A. A. Said, M. Sheik-Bahae, D. J. Hagan, T. H. Wei, J. Wang, J. Young, and E. W. Van Stryland, "Determination of bound-electronic and free-carrier nonlinearities in ZnSe, GaAs, CdTe, and ZnTe," J. Opt. Soc. Am. B **9**, 405 (1992).
26. C. W. Dirk, l. T. Cheng, and M. Kuzyk, "A simplified three-level model describing the molecular third-order nonlinear optical susceptibility," Int. J. Quantum Chem. **43**, 27–36 (1992).
27. E. Zojer, W. Wenseleers, P. Pacher, S. Barlow, M. Halik, C. Grasso, J. W. Perry, S. R. Marder, and J.-L. Brédas, "Limitations of essential-state models for the description of two-photon absorption processes: The example of bis(dioxaborine)-substituted chromophores," J. Phys. Chem. B **108**, 8641–8646 (2004).
28. J.-L. Bredas, C. Adant, P. Tackx, and A. Persoons, "Third-order nonlinear optical response in organic materials: Theoretical and experimental aspects," Chem. Rev. **94**, 243–278 (1994).
29. M. Sheik-bahae, A. A. Said, and E. W. Van Stryland, "High-sensitivity, single-beam n_2 measurements," Opt. Lett. **17**, 955 (1989).
30. E. W. Van Stryland and M. Sheik-bahae, "Z-Scan Measurements of Optical Nonlinearities," Charact. Tech. Tabul. for Org. Nonlinear Materials, M. G. Kuzyk C. W. Dirk, Eds., pp. 655–692 (1998).
31. Y. Gao, W. Wu, D. Kong, L. Ran, Q. Chang, and H. Ye, "Femtosecond nonlinear absorption of ag nanoparticles at surface plasmon resonance," Phys. E **45**, 162–165 (2012).
32. X.-L. Zhang, Z.-B. Liu, X.-C. Li, Q. Ma, X.-D. Chen, J.-G. Tian, Y.-F. Xu, and Y.-S. Chen, "Transient thermal effect, nonlinear refraction and nonlinear absorption properties of graphene oxide sheets in dispersion," Opt. Expr. **21**, 7511–7520 (2013).
33. N. Dong, Y. Li, Y. Feng, S. Zhang, X. Zhang, C. Chang, J. Fan, L. Zhang, and J. Wang, "Optical limiting and theoretical modelling of layered transition metal dichalcogenide nanosheets," Nat. Sci. Reports (2015).
34. J. M. P. Almeida, G. F. B. Almeida, L. Boni, and C. R. Mendonça, "Nonlinear optical properties and femtosecond laser micromachining of special glasses," J. Braz. Chem. Soc. **26**, 2418–2429 (2015).
35. J. Olesiak-Banska, M. Waszkielewicz, K. Matczyszyn, and M. Samoc, "A closer look at two-photon absorption,

absorption saturation and nonlinear refraction in gold nanoclusters," RSC Adv. **6**, 98748 (2016).
36. Y.-X. Zhang and Y.-H. Wang, "Nonlinear optical properties of metal nanoparticles: a review," RSC Adv. **7**, 45129 (2017).
37. C. Torres-Torres, B. Bornacelli, J. Can-Uc, H. G. Silva-Pereyra, L. Rodriguez-Fernandez, M. A. Valos-Borja, J. C. C. Labrada-Delgado, G. J.and Heang-Wong, R. R. Angel-Rojo, and A. Oliver, "Coexistence of two-photon absorption and saturable absorption in ion-implanted platinum nanoparticles in silica plates," Jour. Opt. Soc. Amer. B **35**, 1295–1300 (2018).
38. K. M. McPeak, S. V. Jayanti, S. J. P. Kress, S. Meyer, S. Iotti, A. Rossinelli, and D. J. Norris, "Plasmonic films can easily be better: Rules and recipes," ACS photonics **3**, 326–333 (2015).
39. T. B. Norris, J.-K. Rhee, D. S. Citrin, M. Nishioka, and Y. Arakawa, "Coherent and incoherent dynamics of excitons in semiconductor microcavities," Nuovo Cimento D **17**, 1295–1303 (1995).

Supplementary Material

Contained here are the additional graphics and information associated with the main paper.

First, we briefly discuss the experimental setup described in the paper. In Fig. 13 is the diagrammatic representation of our experimental setup as described in the main text. It is a standard z-scan setup with two arms to simultaneously record both the open and closed aperture data from the sample.

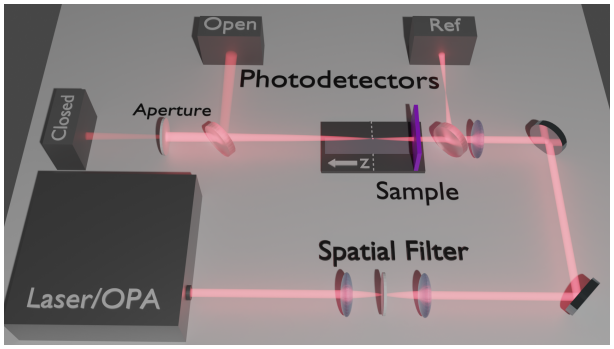

Fig. 13. Experimental z-scan setup for open and closed aperture studies. Both arms of detection are recorded simultaneously by using a beam-splitter at the far-field output of the sample.

As discussed in the main text, here we adopt an illustrative 2-level model expansion to display the effects of an intensity dependent blueshift (τ) embedded in the detuning (δ) of this toy system. The nonlinear parameters in terms of our generalized loss, Γ, and power broadening , P, is given below.

The two-level model expansion discussed in the main text is shown below:

$$n_2 = U(G,\omega)\frac{(\Gamma^2-\delta^2)\tau-\delta P}{(\delta^2+\Gamma^2)^2}$$

$$n_4 = U(G,\omega)\frac{\delta\tau^2\left(\delta^2-3\Gamma^2\right)+\delta P^2-P\tau\left(\Gamma^2-3\delta^2\right)}{\left(\Gamma^2+\delta^2\right)^3}$$

$$n_6 = U(G,\omega)\frac{-\tau^3\left(\Gamma^4-6\Gamma^2\delta^2+\delta^4\right)-\delta P^3+P^2\tau\left(\Gamma^2-5\delta^2\right)+6\delta P\tau^2\left(\Gamma^2-\delta^2\right)}{\left(\Gamma^2+\delta^2\right)^4}$$

which for the limit where $\tau \to 0$ we find the index has alternating nonlinear terms,

$$n-1 = \frac{\delta}{\Gamma^2+\delta^2} - \frac{\delta P}{\left(\Gamma^2+\delta^2\right)^2}I + \frac{\delta P^2}{\left(\Gamma^2+\delta^2\right)^3}I^2 - \frac{\delta P^3}{\left(\Gamma^2+\delta^2\right)^4}I^3$$

When the blueshift parameter is nonzero, the nonlinear terms are no longer resonant at the same detuning. Thus, the largest index shift will correspond to various wavelengths, depending on the relative size of the incident intensity. This simple, illustrative model begins to show why at relatively high incident intensities, the largest change in transmission (and thus the largest change in index) shifts to the blue when compared with the low intensity regime. This can be seen in Fig. 14 in both experiment and theory panels. The linewidth and location of the response changes with incident intensity, as one would expect if there were an intensity dependent blueshift, in our case resulting from optical saturation effectively reducing the vacuum Rabi splitting.

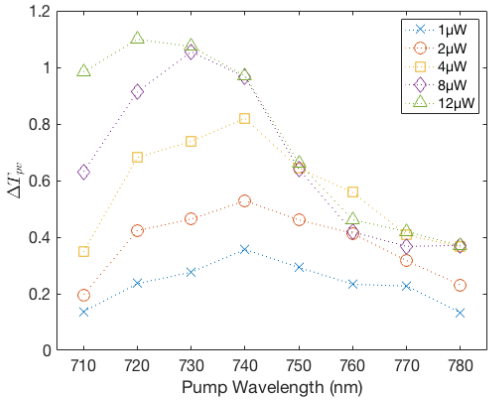

Fig. 14. Experimental change in transmission, peak to valley, for various average power levels.

We now discuss the origin for the data populating Fig. 9. For these data we study the center (z=0) of each z-scan for each power level. This transmission value is recorded for every wavelength that was used in the experiment and theoretical modeling. The result of this is shown in Fig. 15. Each trace shows the evolution of the SA- to RSA-like transition from the blue→red side of the polariton resonance, as discussed in the main text. The point where these traces cross 1 is the corresponding data found in the main text Fig. 9. The inset of the left panel of Fig. 15 shows the experimental crossing of the threshold, reproduced also as the points in Fig. 9.

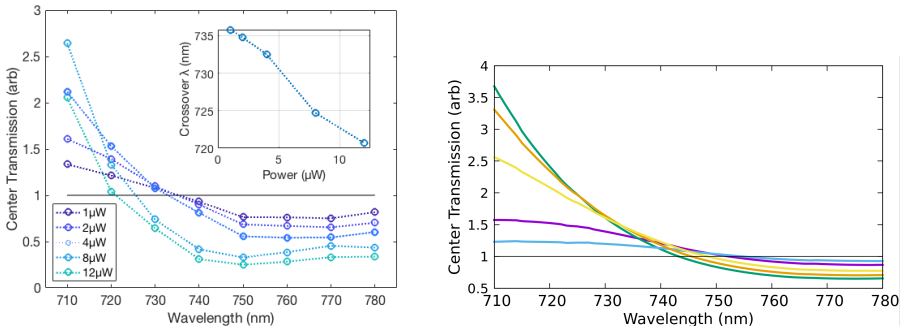

Fig. 15. Center of experimental z-scan for each power level investigated as a function of pump wavelength.(a) Experiment (b) Theory for powers 1, 2.1, 4.3, 6.4, and 8.6 microwatts (blue to green, resp.) power

Lastly, we briefly show the data corresponding to the z-scan of the pure DCDHF-6V film (380nm thick). The open and closed/open traces are shown in Fig. 16. Note the drastically reduced

dynamic range associated with the division, and thus the significantly smaller index change when compared to the polaritonic samples. This is clear evidence of polaritonic enhancement of intensity dependent nonlinear refractive index induced by the polariton resonance.

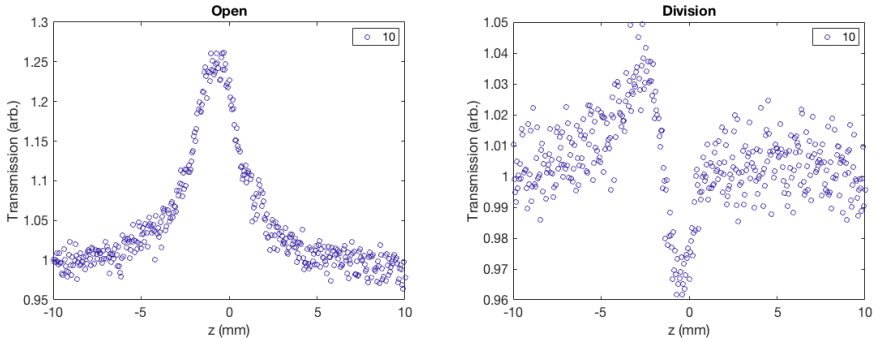

Fig. 16. Experimental z-scan of 370nm thick film of pure DCDHF6V at 10μW of average incident power, pumped using wavelength of 680nm.